Journal of Rare Earths 38 (2020) 376–383

Contents lists available at ScienceDirect

Journal of Rare Earths

journal homepage: http://www.journals.elsevier.com/journal-of-rare-earths

Support interaction of Pt/CeO_2 and Pt/SiC catalysts prepared by nano platinum colloid deposition for CO oxidation☆

Kang Xi, Yong Wang, Kang Jiang, Jing Xie, Ying Zhou, Hanfeng Lu*

Innovation Team of Air Pollution Control, Institute of Catalytic Reaction Engineering, College of Chemical Engineering, Zhejiang University of Technology, Hangzhou 310014, China

ARTICLE INFO

Article history:
Received 23 February 2019
Received in revised form
5 July 2019
Accepted 9 July 2019
Available online 17 August 2019

Keywords:
Nano platinum colloid
CO oxidation
Pt–O–Ce interaction
CeO_2
SiC
Rare earths

ABSTRACT

The interaction between Pt and its various supports can regulate the intrinsic electronic structure of Pt particles and their catalytic performance. Herein, Pt/CeO_2 and Pt/SiC catalysts were successfully prepared via a facile Pt colloidal particle deposition method, and their catalytic performance in CO oxidation was investigated. XRD, TEM, XPS and H_2-TPR were used to identify the states of Pt particles on the support surface, as well as their effect on the performance of the catalysts. Formation of the Pt–O–Ce interaction is one of the factors controlling catalyst activity. Under the oxidative treatment at low temperature, the Pt–O–Ce interaction plays an important role in improving the catalytic activity. After calcining at high temperature, enhanced Pt–O–Ce interaction results in the absence of metallic Pt^0 on the support surface, as evidenced by the appearance of Pt^{2+} species. It is consistent with the XPS data of Pt/CeO_2, and is the main reason behind the deactivation of the catalyst. By contrast, either no interaction is formed between Pt and SiC or Pt nanoparticles remain in the metallic Pt^0 state on the SiC surface even after aging at 800 °C in an oxidizing atmosphere. Thus, the Pt/SiC shows better thermal stability than Pt/CeO_2. The interaction between Pt and the active support may be concluded to be essential for CO oxidation at low temperature, but strong interactions may induce serious deactivation of catalytic activity.

1. Introduction

Supported noble metals, especially Pt-based materials, have been widely used in a variety of catalytic applications, especially three-way catalytic systems, water gas shift reactions, and VOC oxidation.[1–6] Therefore, interest in the development of more economically competitive catalysts for catalytic oxidation of pollutants at ambient temperatures has grown. Over the last several decades, research focus has shifted toward the effects of Pt size and shape, the chemical nature of the support, and the interaction between the support and the metal.[7–11] In this regard, the interaction between Pt and its support has become a popular research topic.[12–16]

The conventional approach to prepare Pt-based catalysts is wet impregnation, which presents the advantages of technical simplicity and reproducible metal ion loading; this technique is widely used in industrial manufacturing.[4,17] Unfortunately, some defects of the process have been reported. For example, the Pt precursor is difficult to adsorb on "inert" support surfaces, resulting in low Pt dispersion and catalyst activity. The adsorption phenomena of the Pt precursor are significantly affected by three important parameters: the isoelectric point of the oxide, the pH of the aqueous solution and the nature of the metal complex.[18–21] Brunelle studied the possible adsorption between several Pt complexes and silica or alumina.[19] For silica, two conditions are required: a solution pH higher than 1, preferably 6, and the use of a metal cationic precursor. For alumina, two conditions are also required: an anionic precursor solution with a pH lower than 8 and a cationic precursor solution with a pH higher than 8. Chen et al. also claimed that the nature of the support could significantly affect the adsorption of the Pt precursor.[4] Based on conventional incipient impregnation methods, the interaction between Pt and its support cannot be easily distinguished from the composite system. The Pt

☆ **Foundation item:** Project supported by the National Natural Science Foundation of China (21506194, 21676255) and the Natural Science Foundation of Zhejiang Province, China (Y16B070025).

* Corresponding author.
E-mail address: luhf@zjut.edu.cn (H.F. Lu).

https://doi.org/10.1016/j.jre.2019.07.012
1002-0721/

particle size, microstructure of the support, and interaction between Pt and the support vary during thermal or redox treatment, thereby increasing the complexity of influencing factors.[22–25]

Organic-phase synthesis is an important method used to precisely control the size and morphology of the Pt nanoparticles.[26–29] Mankin et al. reported the one-pot solution-phase synthesis of Pt nanocubes and nanopods by adjusting the reaction time between 1 and 15 min.[26] Huang et al. reported a general approach to obtain 2-thick Rh-doped Pt nanowires via organic-phase synthesis.[27] Based on this method, a novel strategy to promote the selective adsorption of the Pt precursor on the support surface was proposed; here, the Pt precursor was first synthesized into mono-dispersed Pt nanoparticles and then painted on the support.[29] The Pt loading amount and dispersion of Pt nanoparticles can be effectively controlled in this process. However, whether the nature of the support has any effect on the catalytic activity of Pt nanoparticles and how the interaction between these nanoparticles and the support functions in this method remain unclear.

CeO_2, which is known as an excellent "active support" due to its superior physicochemical properties, has been widely used to build the interaction between Pt and its support; the material features a large number of oxygen vacancies owing to the facile Ce^{4+}/Ce^{3+} redox transition, which presents significant oxygen mobility and storage capacity.[22,30,31] SiC cannot activate oxygen but shows several advantages, including high thermal conductivity, stability, chemical inertness, resistance towards oxidation and mechanical strength; as such, this material can be used as an excellent "inert" support.[32–34] In the present paper, we employed these two representative materials as supports to prepare Pt-based catalysts using the Pt colloidal particle deposition method and investigated the intrinsic catalytic activity of the resulting Pt nanoparticles. The results of this work provide new insights into the preparation of Pt-based catalysts with high activity and thermal stability, as well as a better understanding of the role of Pt nanoparticles in enhancing catalyst performance.

2. Experimental

2.1. Chemical agents

All chemical reagents were obtained from commercial sources and used without further purification. Analytical grade cerium nitrate hexahydrate ($Ce(NO_3)_3\cdot 6H_2O$; 99.5%) was purchased from Sinopharm Chemical Reagent Co., Ltd. Silicon carbide (SiC; 99%), oleylamine (OAm; >80%), oleic acid (OA; 99.5%), 1-octadecene (ODE; >90%) and dinitrodiammineplatinum ammoniacal ($Pt(NH_3)_2(NO)_2$; 59%) were purchased from Shanghai Aladdin Biochemical Technology Co., Ltd.

2.2. Catalyst preparation

2.2.1. Preparation of CeO_2 support

The CeO_2 support was synthesized through ammonia coprecipitation. Briefly, the required amount of $Ce(NO_3)_3\cdot 6H_2O$ was dissolved in deionized water, and a suspension was achieved by dropwise addition of 1 mol/L $NH_3\cdot H_2O$ until pH = 9–10. The precipitate obtained was isolated by filtration, washed thrice with deionized water, and dried at 110 °C for 12 h. Finally, the sample was calcined at 500 °C for 3 h. The sintered CeO_2 was calcined at 800 °C for 5 h.

2.2.2. Synthesis of Pt colloidal nanoparticles

In a typical synthesis of Pt colloidal particles, 20 mg of $Pt(NH_3)_2(NO)_2$, 10 mL of 1-octadecene, 5 mL of oleylamine and 5 of oleic acid were mixed together in a three-necked round-bottomed flask with a capacity of 50 ml and then heated at 70 °C for 5 min to form a homogeneous yellow solution. The solution was then heated at 200 °C for 2 h under the protection of N_2. After the solution was cooled to room temperature, the product was precipitated by ethanol, washed thrice with hexane, and re-dispersed in hexane. Finally, black Pt colloidal particles were obtained.

2.2.3. Preparation of Pt/CeO_2 and Pt/SiC catalysts

In a typical synthesis, the appropriate amount of as-prepared Pt colloidal nanoparticle solution was poured directly onto 1 g of either CeO_2 or SiC at room temperature and stirred for 10 min. The resultant mixture was then slowly heated under constant stirring until complete evaporation of hexane. The solid product was further dried at 110 °C overnight. Subsequently, the dried sample was calcined at T (T = 200, 400, 600 or 800 °C) for 3 h in flowing air to obtain the Pt-based catalysts. The loading of Pt on the supports was fixed at 0.2 wt%, and the final samples prepared using CeO_2 and SiC as supports were respectively denoted as Pt/CeO_2-T and Pt/SiC-T (T = 200, 400, 600, or 800 °C, representing the calcination temperature).

2.3. Catalyst characterization

The structural features of all catalysts were characterized by powder XRD. XRD patterns were recorded on a diffractometer (ARLSCINTAG X'TRA) operated at 45 and 30 mA using nickel-filtered Cu-Kα radiation. Diffractograms were registered between 20° and 80° (2θ) with a 0.02° step.

The specific surface areas of samples were determined by N_2 adsorption measurements at −196 °C using the Brunauer-Emmett-Teller (BET) method and a micropore porosity analyzer (3Flex, Micromeritics, USA). Samples were pretreated under vacuum at 200 °C for 8 h prior to measurement.

The reducibility of the catalysts was studied by H_2-TPR experiments on a chemisorption analyzer (FINESORB-3010E, Fantai, China). Catalysts (100 mg) were pretreated in a U-shaped quartz reactor at 200 °C for 1 h and subsequently cooled to 100 °C under an air flow (30 mL/min). Then, the catalyst bed was subjected to a flow (30 mL/min, 5% H_2 in Ar) at 100 °C for 20 min, followed by heating at a constant rate (10 °C/min) up to 750 °C. Finally, the catalyst was cooled under an Ar flow (30 mL/min). Hydrogen consumption was monitored using a thermal conductivity detector operating at 60 °C and 60 mA.

A Kratos AXIS Ultra DLD photoelectron spectrometer with a monochromatized microfocused Al X-ray source was used for XPS measurements (Shimadzu Scientific Instruments, Japan). The charging of the samples was corrected by setting the binding energy of adventitious carbon (C 1s) to 284.6 eV. Prior to measurement, the powdered samples were pressed into self-supporting disks, loaded into a sub chamber, and then evacuated at 25 °C for 4 h.

The micromorphology and actual composition of the samples were determined with a HRTEM (Tecnai G2 F30 S-Twin 300 kV, Philips-FEI, Netherlands) microscope coupled to an EDS analyzer.

2.4. Catalytic test

The activity of the catalysts for oxidation of CO was measured using a continuous-flow fixed-bed reactor system. In a typical reaction, 100 mg of the as prepared Pt/CeO_2 sample (mixed with 200 mg of silicon) was directly placed in a U-shaped, quartz microreactor with an internal diameter of 4 mm. The feed flow through the reactor was 1% CO and 21% O_2 balanced with N_2. The CO oxidation reaction was performed under a total gas flow rate of 42 mL/min to maintain a weight hourly space velocity of

25000 mL/(g·h). Kinetic data were taken after 10 min of streaming at each reaction temperature. The concentration of CO was analyzed on-line by a gas chromatograph (GC-2014, Shimadzu, Japan) equipped with a TCD at a given temperature for 5 times after stabilization for 10 min.

The turnover frequency (TOF) of CO oxidation was calculated on the basis of the dispersion of Pt nanoparticles on the catalyst surface and conversion rate of CO is

$$\mathrm{TOF} = X_{\mathrm{CO}} \cdot F_{\mathrm{CO}} \cdot M_{\mathrm{Pt}} / (m_{\mathrm{cat}} \cdot X_{\mathrm{Pt}} \cdot D_{\mathrm{Pt}}) \quad (1)$$

where X_{CO} is the CO conversion at a certain temperature, F_{CO} the flow rate of CO in units of mol/s, m_{cat} the amount of catalyst, X_{Pt} the mass fraction of Pt in catalysts and D_{Pt} the dispersion of Pt. TOF represents the conventional calculation of CO frequency based on metal dispersion.

3. Results and discussion

3.1. Characterization of the Pt colloidal particles

To obtain a stable Pt colloid, preparing monodispersed Pt nanoparticles of the proper size is key. The size and morphology of the Pt nanoparticles were examined by TEM and HRTEM, as shown in Fig. 1. From Fig. 1(a) and (b), the Pt nanoparticles in the parent solution are monodispersed and spheroidal in shape. A lattice spacing of 0.23 nm corresponding to the (111) plane of Pt could be observed on HRTEM images, thereby suggesting the existence of Pt cubes. The distribution of cracked product fractions are depicted in the HRTEM image in Fig. 1(e). The average size of the Pt nanoparticles is 5.1 nm, and the particles show low aggregation and a narrow size distribution. The monodispersed structure of the Pt nanoparticles promotes their dispersal in liquid. Fig. 1(d) reveals that the Pt colloidal particles are extremely stable and could be stored for 2 months without delamination or sol destruction.

Pt/SiC and Pt/CeO_2 catalysts with 0.2 wt% Pt were prepared by the Pt colloidal particle deposition method, and Fig. 2(a1–a7) show the TEM and HRTEM images and EDS mappings of Pt/SiC-200. A homogeneous Pt nanoparticle distribution can be clearly observed over Pt/SiC, and the metal presents a particle size of 5 nm (Fig. 2(a1–a3)). The EDS mappings (Fig. 2(a4–a7)) confirm the observed homogeneous Pt distribution. These findings indicate that high dispersion of Pt nanoparticles on the "inert" support can be effectively achieved and the particle size can be easily controlled by the selected preparation process. After Pt loading, the number of Pt nanoparticles significantly decreases, and the grain size of Pt increases, as shown in Fig. 2(b1–b3), probably as a result of the heating treatment. The EDS mappings (Fig. 2(b7)) further confirm the agglomeration of Pt nanoparticles. Consequently, the Pt nanoparticles are unstable on the SiC surface, and their size increases to 10 nm under the high heating treatment (Fig. 2(b3)).

TEM and HRTEM images and the EDS mapping of the Pt/CeO_2 catalysts calcined at 200 and 800 °C are shown in Fig. 3. Discriminating the Pt nanoparticles between Fig. 3(a1) and (b1) is difficult because the atomic number of Ce is 58 whereas that of Si is 14, and the contrast of the CeO_2 support hinders identification of

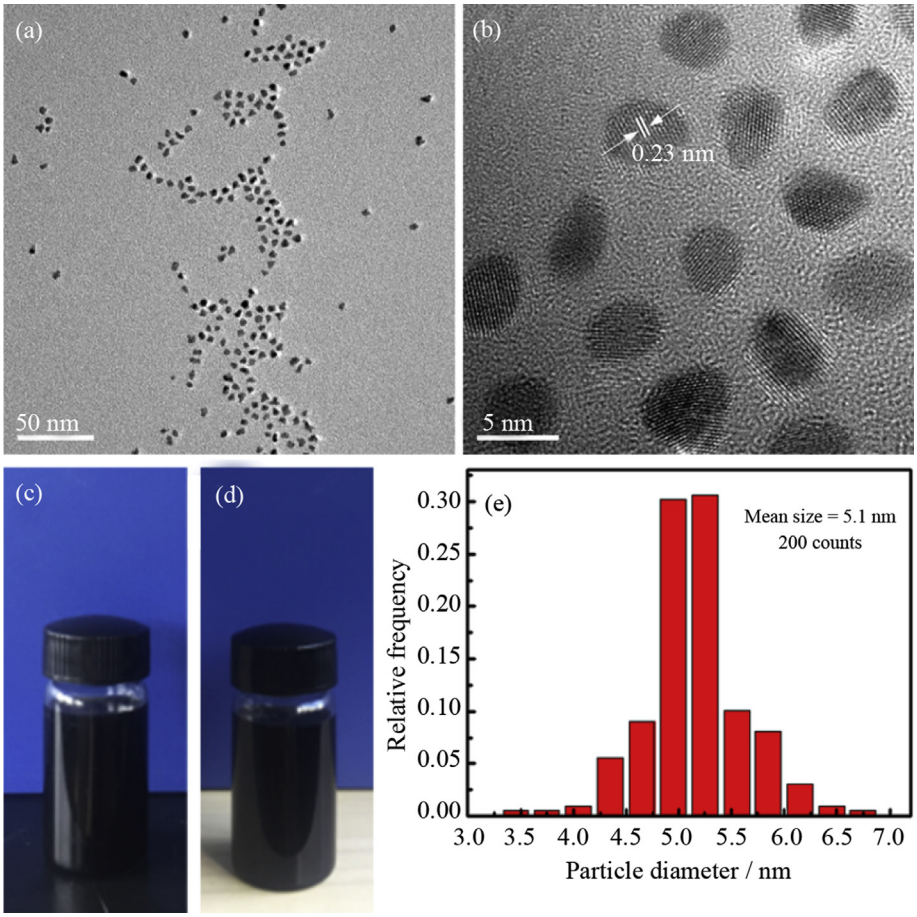

Fig. 1. Photographs of the nano platinum colloid (c) and the sample after two months storage (d). TEM image (a), HRTEM image (b) and size histograms (e) of the Pt nanoparticles.

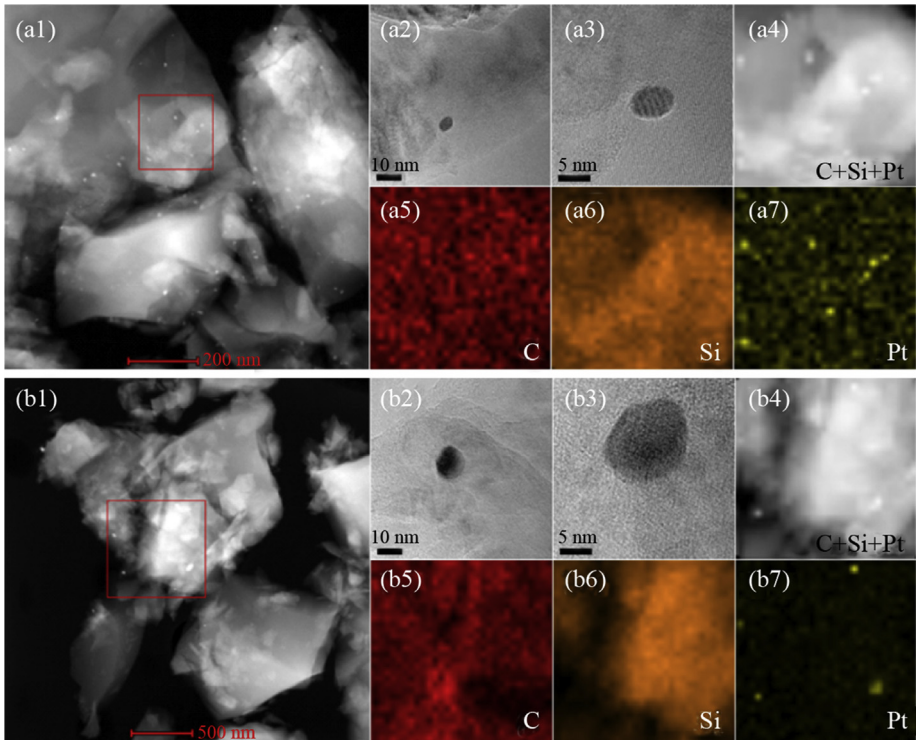

Fig. 2. TEM images and EDS mapping of Pt/SiC-200 (a1–a3, a4–a7) and Pt/SiC-800 (b1–b3, b4–b7).

large Pt particles in these images.[35,36] The HRTEM images in Fig. 3(a2,a3) as well as the EDS mapping in Fig. 3(a7), clearly show the presence of Pt. This observation agrees with the extraordinarily high dispersion of Pt nanoparticles on the surface of CeO_2 during the preparation of the catalyst.[23,37,38] Compared with Pt/SiC-800, Pt/CeO_2-800 shows no agglomeration of Pt nanoparticles. CeO_2 could play an important role in stabilizing in Pt nanoparticles against sintering under an oxidative atmosphere at high temperature, according to results published in literature.[39–41]

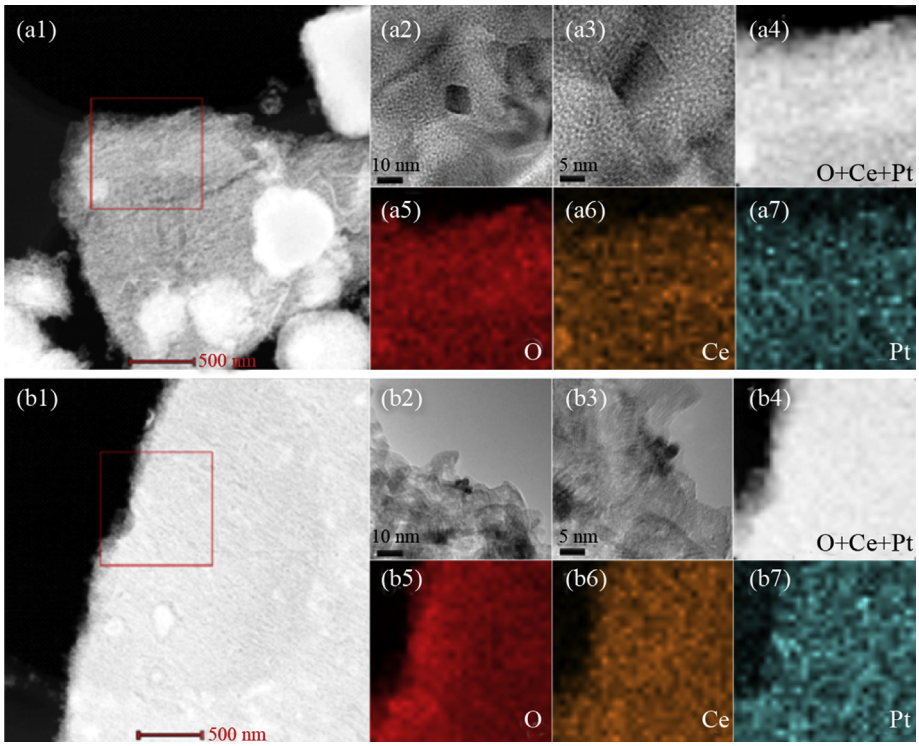

Fig. 3. TEM images and EDS mapping of Pt/CeO_2-200 (a1–a3, a4–a7) and Pt/CeO_2-800 (b1–b3, b4–b7).

3.2. Characterization of the catalysts

Fig. 4 shows the XRD patterns of the Pt/CeO_2 and Pt/SiC samples after treatment at various temperatures. The crystallite sizes as calculated from the Scherrer equation are summarized in Table 1. While the Pt/CeO_2 catalysts obtained after treatment at various temperatures display a typical cubic fluoride CeO_2 crystal phase (JCPDS Card No. 34-0394), the Pt/SiC catalysts display a hexagonal SiC crystal phase (JCPDS Card No. 74-1302). No diffraction peak related to Pt or PtO_x phases (at 40°) could be observed in the XRD patterns, which could be attributed to the low metal loading content.[6,22,42] When Pt/CeO_2 is oxidized at 800 °C, its pore structure collapses, and the mean pore size increases from 13.3 to 18.3 nm. By comparison, Pt/SiC maintains its structure even upon oxidation at 800 °C. This finding is supported by the BET surface area data in Table 1, which shows that the surface area of Pt/CeO_2 steadily decreases from 63 to 15 m^2/g as the calcination temperature increases from 200 to 800 °C. The change in textural property of Pt/SiC is completely different from that of Pt/CeO_2; the BET surface area of the former remains fairly stable even after treatment at 800 °C. Thus, the physical structure of Pt/SiC is more stable than that of Pt/CeO_2.

3.3. Reduction behavior and chemical states

The reducibilities of the Pt/CeO_2 and Pt/SiC samples were investigated using H_2-TPR measurements, and the corresponding reduction profiles are presented in Fig. 5. For pure CeO_2, two broad peaks could be observed in the range of 300–550 and 650–850 °C, representing the reduction of surface and bulk oxygen, respectively. After Pt loading, the Pt/CeO_2 samples demonstrate a significant decrease in reduction temperature and increase in H_2 consumption at low temperatures. This change is probably caused by the formation of the Pt–O–Ce interaction, which can activate lattice oxygen on the surface of CeO_2 and promote the low-temperature reducibility of the catalysts.[14,43] As the oxidation temperature increases, the Pt–O–Ce interaction becomes stronger and is able to activate more lattice oxygen on the surface of CeO_2, thereby causing enhanced surface reduction.[6,38,44] As shown in Table 2, compared with that of Pt/CeO_2-200, the consumption of surface reduction peaks increases from 76 to 391 μmol/g for Pt/CeO_2-600 and 133 μmol/g for Pt/CeO_2-800. Because of the thermal sintering of CeO_2, the H_2 consumption of Pt/CeO_2-800 is lower than that of Pt/

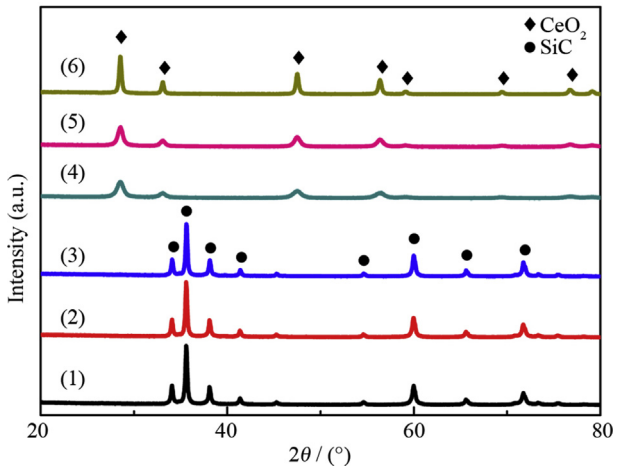

Fig. 4. XRD patterns of the catalysts. (1) Pt/SiC-200; (2) Pt/SiC-600; (3) Pt/SiC-800; (4) Pt/CeO_2-200; (5) Pt/CeO_2-600; (6) Pt/CeO_2-800.

Table 1
Textural parameters of various catalysts.

Sample	S_{BET} (m^2/g)	V_{pore} (cm^3/g)	Pore size (nm)	Crystallite size (nm)
Pt/CeO_2-200	63	0.21	13.3	9.2
Pt/CeO_2-600	48	0.17	14.5	12.4
Pt/CeO_2-800	15	0.07	18.3	33.2
Pt/SiC-200	12	0.03	11.0	51.5
Pt/SiC-600	10	0.03	11.7	51.2
Pt/SiC-800	11	0.04	14.2	53.8

CeO_2-600. In summary, the H_2-TPR study clearly demonstrates that the Pt–O–Ce interaction actives the lattice oxygen on the surface of CeO_2 and promotes the reducibility of the corresponding catalysts. Interestingly, the bulk reduction peak of ceria in all samples at 800 °C is not affected by the presence of Pt or the calcination temperature, which illustrates that the Pt–O–Ce interaction can only activate the oxygen on the surface of CeO_2. Fig. 5 reveals no H_2 consumption peak or PtO_x reduction peak for both the SiC support and Pt/SiC catalysts, likely because SiC cannot supply active oxygen for H_2 consumption. This finding indirectly indicates that no interaction is formed between Pt and SiC and that the Pt nanoparticles on the SiC surface are in the Pt^0 state, which corresponds well to the XPS results.

To understand the effect of high heat treatment on the Pt nanoparticles, XPS measurements were employed to probe the chemical states of the Pt species in the Pt/CeO_2 and Pt/SiC catalysts. Fig. 6 presents the XPS spectra of Pt 4f for Pt/SiC and Pt/CeO_2, and the data of surface Pt concentrations are listed in Table 3. As seen in this figure, the Pt/CeO_2-200 catalyst shows four peaks at 70.9, 71.9, 74.2 and 75.2 eV. According to the literature, the BEs for Pt^0 $4f_{7/2}$ and $4f_{5/2}$ are 71.1 and 74.4 eV, respectively.[2,35,43] The Pt^{2+} peaks at +1.9 eV relative to the peak position of Pt^0 are located at 73.0 and 76.3 eV. Thus, the peaks of Pt/CeO_2-200 at 70.9 and 74.2 eV can be assigned to Pt^0 $4f_{7/2}$ and $4f_{5/2}$, respectively. The peaks at 71.9 and 75.2 eV shift by +1.0 eV from those of Pt^0 $4f_{7/2}$ and $4f_{5/2}$ (70.9 and 74.2 eV, respectively), instead of shifting by +2.0 eV to form Pt^{2+} species. This result indicates that, because of the Pt–O–Ce interaction, Pt nanoparticles not only exist on the CeO_2 surface as Pt^0 species but also partly participate in the formation of the Pt–O–Ce bond, resulting in the presence of unanticipated $Pt^{\delta+}$ species.[35,45] For the Pt/CeO_2-800 catalyst, two single peaks at 72.8 and 76.1 eV are observed, and these peaks correspond well to Pt^{2+} species. That is, all of the Pt nanoparticles participate in the formation of the Pt–O–Ce bond in the Pt/CeO_2-800 catalyst, resulting in an abundance of Pt^{2+} species on the support surface. The presence of Pt–O–Ce interactions in the Pt/CeO_2 catalyst can be explained as follows: If no Pt–O–Ce interaction occurs between Pt and CeO_2, the former decomposes into metallic Pt during oxidative treatment at high temperatures according to the thermodynamic calculations. This decomposition phenomenon can also be observed in Pt/Al_2O_3 catalysts.[35,41] By contrast, the Pt 4f line profile of all Pt/SiC catalysts can be fitted to two peaks appearing at 71.2 and 72.6 eV, which, as previously stated, can be explicitly assigned to Pt^0 $4f_{7/2}$ and $4f_{5/2}$, respectively. Pt^0 appears to be the dominant species for all Pt/SiC catalysts, which means no obvious interaction occurs between Pt and SiC.

3.4. Catalysts activity test

Fig. 7 presents the activities of the catalysts for CO oxidation as a function of reaction temperature. Table 4 lists the temperatures required to achieve removal efficiencies of 50% ($T_{50\%}$) and 100% ($T_{100\%}$), as well as the TOF_{Pt} values, which are calculated based on

Table 2
H_2-TPR characterization of CeO_2 and Pt/CeO_2 samples.

Samples	Low-temperature reduction peak (°C)	Hydrogen consumption (μmol/g)
CeO_2	300–600	335
Pt/CeO_2-200	120–290	76
Pt/CeO_2-600	170–290	391
Pt/CeO_2-800	290–380	133

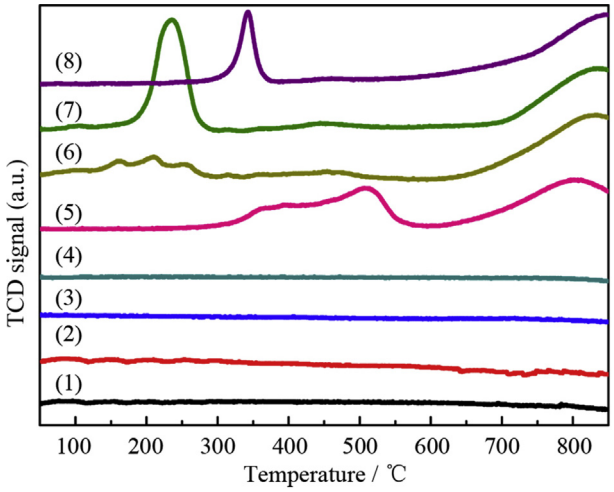

Fig. 5. H_2-TPR profiles of the catalysts. (1) SiC (2) Pt/SiC-200; (3) Pt/SiC-600; (4) Pt/SiC-800; (5) CeO_2; (6) Pt/CeO_2-200; (7) Pt/CeO_2-600; (8) Pt/CeO_2-800.

the Pt dispersion at 100 and 160 °C. The conversion of CO over pure CeO_2 is around 100% at 350 °C; by contrast, SiC shows no activity at this temperature. Ceria can form active oxygen on its surface to help catalyze CO oxidation.[45–48] Compared with pure CeO_2, the Pt/CeO_2 catalysts exhibit better catalytic performance. In particular, the $T_{50\%}$ and $T_{100\%}$ of Pt/CeO_2-200 are equal to 125 and 135 °C, respectively, which are as low as 151 and 225 °C compared with those of pure CeO_2. According to the H_2-TPR results, the Pt–O–Ce interaction between Pt and ceria is beneficial for CO oxidation because it promotes activation of oxygen on the CeO_2 surface, which provides ideally synergistic condition for CO oxidation.[2,38]

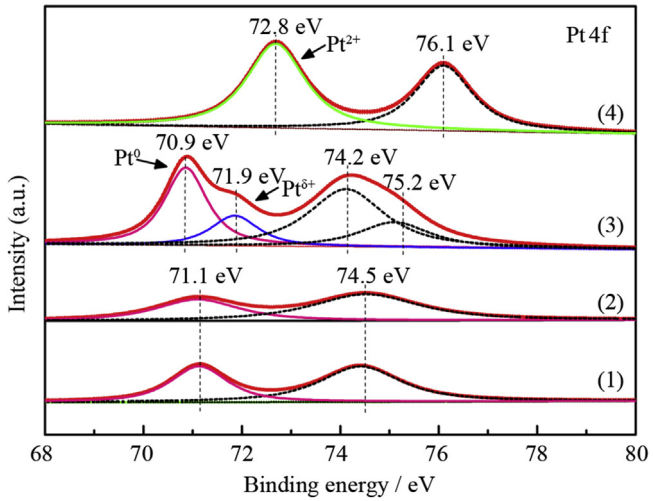

Fig. 6. XPS patterns of the catalysts. (1) Pt/SiC-200; (2) Pt/SiC-800; (3) Pt/CeO_2-200; (4) Pt/CeO_2-800.

Table 3
XPS results of various samples.

Samples	Pt loading (wt%)	Species
Pt/SiC-200	0.21	Pt^0
Pt/SiC-800	0.20	Pt^0
Pt/CeO_2-200	0.22	$Pt^0 + Pt^{\delta+}$
Pt/CeO_2-800	0.21	Pt^{2+}

The activity of the Pt/CeO_2 catalysts decreases slightly when the temperature is raised from 200 to 800 °C. Catalyst activity shows the order: Pt/CeO_2-200 > Pt/CeO_2-400 > Pt/CeO_2-600 > Pt/CeO_2-800, and CO conversion over these catalysts reveals large differences. The $T_{50\%}$ and $T_{100\%}$ of Pt/CeO_2-200 are 125 and 135 °C respectively, while those of Pt/CeO_2-600 and Pt/CeO_2-800 are 225 and 255 °C and 240 and 360 °C, respectively. The calcination temperature can thus be concluded to be a critical parameter influencing the Pt/CeO_2 catalysts. Excessively high temperatures may bring about deactivation of the catalyst, especially in Pt/CeO_2-600 and Pt/CeO_2-800. To reveal the mechanism of deactivation of the Pt/CeO_2 catalysts, detailed analysis was carried out. According to published findings, sintering of ultrafine Pt crystallites dispersed on SiO_2 and Al_2O_3 supports under high calcination temperatures may result in drastic decrease in catalytic activity.[40,49] In the Pt/CeO_2 catalysts, however, no sintering phenomenon occurs in the agglomerated powder and nanoparticle's size, according to Fig. 3. Thus, sintering of Pt nanoparticles is not the main reason behind the deactivation of the Pt/CeO_2 catalysts. Besides, we proved that the structure of the Pt/CeO_2 catalysts is unstable according to XRD and BET results, and their specific surface area decreased rapidly with increasing heat treatment temperature.

To avoid the influence caused by structural changes, comparative experiments were conducted. In this case, the CeO_2 support was first calcined at 800 °C, after which the Pt supported catalysts were prepared via the same procedure described in the previous section. The final catalysts were denoted as $Pt/CeO_2(800)$-T (T = 200, 400, 600, 800 °C). The performance of the catalysts is

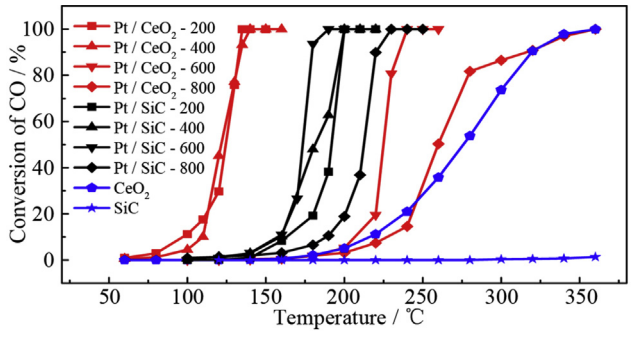

Fig. 7. Conversion of CO over SiC, CeO_2, Pt/SiC and Pt/CeO_2 catalysts (Feed gas: 1% CO, 21% O_2, balance N_2, WHSV = 25000 ml/(g·h)).

Table 4
Catalytic performances for various catalysts.

Sample	Catalytic activity		TOF_{Pt}[a] (s^{-1})	TOF_{Pt}[b] (s^{-1})
	$T_{50\%}$ (°C)	$T_{100\%}$ (°C)		
Pt/SiC-200	195	200	–	0.11
Pt/SiC-400	182	200	–	0.14
Pt/SiC-600	173	190	–	0.15
Pt/SiC-800	215	230	–	0.08
CeO_2	276	360	–	–
Pt/CeO_2-200	125	135	0.15	–
Pt/CeO_2-400	123	140	0.06	–
Pt/CeO_2-600	225	240	–	0.75×10^{-2}
Pt/CeO_2-800	255	360	–	0.17×10^{-2}

[a] The TOF values were calculated at 100 °C.
[b] The TOF values were calculated at 160 °C.

shown in Fig. 8. The activity of the Pt/CeO_2(800) catalysts demonstrates the same change trend as the Pt/CeO_2 catalysts under high heat treatment temperatures, and obvious deactivation could also be observed. Therefore, the structural instability of the Pt/CeO_2 catalysts is not the main reason behind their deactivation. The Pt–O–Ce interaction is formed between Pt and CeO_2 according to H_2-TPR results, and the interaction becomes stronger as the oxidation temperature increases from 200 to 800 °C, as evidenced by the shift in surface reduction peak of Pt/CeO_2 in the H_2-TPR plots. The XPS patterns show that the Pt–O–Ce interaction exerts an obvious influence on the state of the Pt nanoparticles. For Pt/CeO_2-200, a relatively weak Pt–O–Ce interaction is formed between Pt and CeO_2; thus, the Pt nanoparticles not only participate in the formation of the Pt–O–Ce bond, which provides the active oxygen for CO oxidation, but also exists on the CeO_2 surface as Pt^0 species, which provide the main sites for CO adsorption. Given these characteristics, the Pt/CeO_2 catalysts show good activity under low thermal treatment. After calcination at high temperature, however, stronger Pt–O–Ce interactions result in the absence of Pt^0 species, and all of the Pt nanoparticles participate in the formation of the Pt–O–Ce bond. Abundant surface Pt^0 is essential to provide suitable active sites for facile oxidation of CO.[24] Thus, the absence of surface Pt^0 induces the obvious deactivation of Pt/CeO_2-800.

Fig. 7 illustrates that the Pt/CeO_2 catalysts have higher activity than the Pt/SiC catalysts calcined at low temperature (200 and 400 °C), thereby suggesting the promoting effect of the Pt–O–Ce interaction. The $T_{50\%}$ and $T_{100\%}$ of Pt/CeO_2-200 are equal to 125 °C and 135 °C, respectively, which are low as 70 and 65 °C compared with those of Pt/SiC-200. After calcination at 800 °C, however, the opposite activity is observed, and the $T_{50\%}$ and $T_{100\%}$ of Pt/SiC-800 are equal to 215 and 230 °C, respectively, while those of Pt/CeO_2-800 are 255 and 360 °C. The Pt/SiC catalysts are seemingly more thermodynamically stable than the Pt/CeO_2 catalysts, even under high-temperature heat treatment. The slight decrease in activity compared with that of Pt/SiC-200 is due to the agglomeration of Pt nanoparticles (Fig. 3). No interaction appears to be formed between Pt and SiC, and Pt nanoparticles remain in the Pt^0 state on the SiC surface even after aging at 800 °C in an oxidizing atmosphere. This abundance of surface Pt^0 allows Pt/SiC to show better thermal stability than the Pt/CeO_2 catalysts.

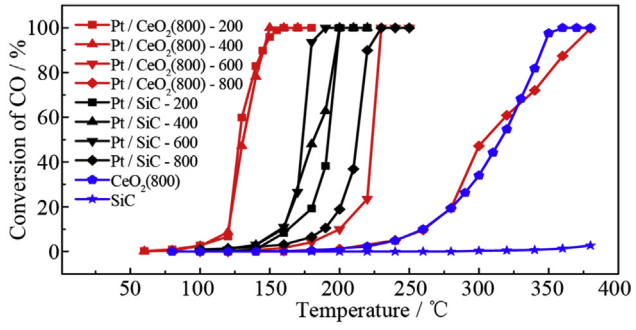

Fig. 8. Conversion of CO over SiC, CeO_2 (800), Pt/SiC and Pt/CeO_2 (800) catalysts (Feed gas: 1% CO, 21% O_2, balance N_2, WHSV = 25000 ml/(g·h)).

4. Conclusions

In this study, Pt/CeO_2 and Pt/SiC catalysts were successfully synthesized via a simple Pt colloidal particle deposition method. Formation of the Pt–O–Ce interaction can be observed from the H_2-TPR and XPS results, and findings reveal that this interaction does not always increase catalyst activity. Under low thermal treatment (200 and 400 °C), the Pt–O–Ce interaction plays an important role in improving catalytic activity by activating the surface oxygen of CeO_2. After calcining at high temperature (600 and 800 °C), intensification of the Pt–O–Ce interaction results in the absence of surface Pt^0, which provides the main sites for CO adsorption, and the Pt/CeO_2-800 catalyst is obviously deactivated. While no interaction is formed between Pt and SiC, Pt/SiC-200 shows lower activity than the Pt/CeO_2-200 catalyst. After calcination at 800 °C in an oxidizing atmosphere, however, an abundance of surface Pt^0 endows Pt/SiC-800 with better thermal stability than Pt/CeO_2-800. These results demonstrate that the interaction between Pt and its active support presents a double-edged sword for CO oxidation, and strong interactions may induce serious deactivation of Pt-based catalysts.

References

1. Oran U, Uner D. Mechanisms of CO oxidation reaction and effect of chlorine ions on the CO oxidation reaction over Pt/CeO_2 and Pt/CeO_2/γ-Al_2O_3 catalysts. *Appl Catal B*. 2004;54(3):183.
2. Bera P, Gayen A, Hegde MS, Lalla NP, Spadaro L, Frusteri F, et al. Promoting effect of CeO_2 in combustion synthesized Pt/CeO_2 catalyst for CO oxidation. *J Phys Chem B*. 2003;107(25):6122.
3. Park JE, Kim KB, Kim Y, Song KS, Park ED. Effect of Pt particle size on propane combustion over Pt/ZSM-5. *Catal Lett*. 2013;143(11):1132.
4. Chen F, Wang F, Li Q, Cao CY, Zhang X, Ma H, et al. Effect of support (Degussa P25 TiO_2, anatase TiO_2, γ-Al_2O_3, and AlOOH) of Pt-based catalysts on the formaldehyde oxidation at room temperature. *Catal Commun*. 2017;99:39.
5. Yang TF, Huo Y, Liu Y, Rui ZB, Ji HB. Efficient formaldehyde oxidation over nickel hydroxide promoted Pt/γ-Al_2O_3 with a low Pt content. *Appl Catal B*. 2017;200:543.
6. Peng RS, Sun XB, Li SJ, Chen LM, Fu ML, Wu JL, et al. Shape effect of Pt/CeO_2 catalysts on the catalytic oxidation of toluene. *Chem Eng J*. 2016;306(15):1234.
7. Chen JY, Lim B, Lee EP, Xia YN. Shape-controlled synthesis of platinum nanocrystals for catalytic and electrocatalytic applications. *Nano Today*. 2009;4(1):81.
8. Leong GJ, Schulze MC, Strand MB, Maloney D, Frisco SL, Dinh HN, et al. Shape-directed platinum nanoparticle synthesis: nanoscale design of novel catalysts. *Appl Organomet Chem*. 2014;28(1):1.
9. Wang L, Yue HQ, Hua ZL, Wang HY, Li XB, Li LC. Highly active Pt/Na_xTiO_2 catalyst for low temperature formaldehyde decomposition. *Appl Catal B*. 2017;219:301.
10. Wan J, Ran R, Li M, Wu XD, Weng D. Effect of acid and base modification on the catalytic activity of Pt/Al_2O_3 for propene oxidation. *J Mol Catal A Chem*. 2014;383–384:194.
11. Pazmiño JH, Shekhar M, Williams WD, Akatay MC, Miller JT, Delgass WN, et al. Metallic Pt as active sites for the water–gas shift reaction on alkali-promoted supported catalysts. *J Catal*. 2012;286:279.
12. Jung S, Suzuki A, Tsuboi H, Hatakeyama N, Endou A, Takaba H, et al. An elucidation of the interaction between Pt particles and CeO_2 surfaces using tight-binding quantum chemistry method. *Top Catal*. 2010;53(7–10):700.
13. Li H, Wang Y, Chen X, Liu S, Zhou Y, Zhu QL, et al. Preparation of metallic monolithic Pt/FeCrAl fiber catalyst by suspension spraying for VOCs combustion. *RSC Adv*. 2018;8(27):14806.
14. Gao YX, Wang WD, Chang SJ, Huang WX. Morphology effect of CeO_2 support in the preparation, metal-support interaction, and catalytic performance of Pt/CeO_2 catalysts. *ChemCatChem*. 2013;5(12):3610.
15. Ivanova AS, Slavinskaya EM, Gulyaev RV, Zaikovskii VI, Stonkus OA, Danilova IG, et al. Metal-support interactions in Pt/Al_2O_3 and Pd/Al_2O_3 catalysts for CO oxidation. *Appl Catal B*. 2010;97(1–2):57.

16. Zhu AM, Zhou Y, Wang Y, Zhu QL, Liu HY, Zhang ZK, et al. Catalytic combustion of VOCs on Pt/CuMnCe and Pt/CeY honeycomb monolithic catalysts. *J Rare Earths*. 2018;36(12):1272.
17. Winkler A, Ferri D, Aguirre M. The influence of chemical and thermal aging on the catalytic activity of a monolithic diesel oxidation catalyst. *Appl Catal B*. 2009;93(1–2):177.
18. Aristizábal A, Contreras S, Divins NJ, Llorca J, Medina F. Pt–Ag/activated carbon catalysts for water denitration in a continuous reactor: incidence of the metal loading, Pt/Ag atomic ratio and Pt metal precursor. *Appl Catal B*. 2012;127:351.
19. Brunelle JP. Preparation of catalysts by adsorption of metal complexes on mineral oxides. *Stud Surf Sci Catal*. 1979;3:211.
20. Wang YD, Tao ZC, Wu BS, Xu J, Huo CF, Li K, et al. Effect of metal precursors on the performance of Pt/ZSM-22 catalysts for n-hexadecane hydroisomerization. *J Catal*. 2015;322:1.
21. Anderson JR. Characterization of catalysts (structure of metallic catalysts). *Science*. 1976;191(4231):1043.
22. Meher SK, Cargnello M, Troiani H, Montini T, Rao GR, Fornasiero P. Alcohol induced ultra-fine dispersion of Pt on tuned morphologies of CeO_2 for CO oxidation. *Appl Catal B*. 2013;130–131:121.
23. Reber AC, Khanna SN. Effect of embedding platinum clusters in alumina on sintering, coking, and activity. *J Phys Chem C*. 2017;121(39):21527.
24. Zheng B, Liu G, Geng LL, Cui JY, Wu SJ, Wu P, et al. Role of the FeO_x support in constructing high-performance Pt/FeO_x catalysts for low-temperature CO oxidation. *Catal Sci Technol*. 2016;6(5):1546.
25. Kang SB, Hazlett M, Balakotaiah V, Kalamaras C, Epling W. Effect of Pt:Pd ratio on CO and hydrocarbon oxidation. *Appl Catal B*. 2018;223:67.
26. Mankin MN, Mazumder V, Sun SH. One-pot synthesis of Pt nanocubes and nanopods via burst nucleation and controlled secondary growth. *Chem Mater*. 2011;23(2):132.
27. Huang HW, Li K, Chen Z, Luo LH, Gu YQ, Zhang DY, et al. Achieving remarkable activity and durability toward oxygen reduction reaction based on ultrathin Rh-doped Pt nanowires. *J Am Chem Soc*. 2017;139(24):8152.
28. Peng ZM, Yang H. Designer platinum nanoparticles: control of shape, composition in alloy, nanostructure and electrocatalytic property. *Nano Today*. 2009;4(2):143.
29. Jia CJ, Schüth F. Colloidal metal nanoparticles as a component of designed catalyst. *Phys Chem Chem Phys*. 2011;13(7):2457.
30. Li L, Qian Y, Yang JJ, Tan XY, Dai Z, Jin YX, et al. A novel structural design of hybrid nanotube with CNTs and CeO_2 supported Pt nanoparticles with improved performance for methanol electro-oxidation. *Int J Hydrogen Energy*. 2016;41(22):9284.
31. Ozawa M, Okouchi T, Haneda M. Three way catalytic activity of thermally degenerated Pt/Al_2O_3 and Pt/CeO_2–ZrO_2 modified Al_2O_3 model catalysts. *Catal Today*. 2015;242:329.
32. Oi-Uchisawa J, Obuchi A, Enomoto R, Xu JY, Nanba T, Liu ST, et al. Oxidation of carbon black over various Pt/MO_x/SiC catalysts. *Appl Catal B*. 2001;32(4):257.
33. Fang L, Huang XP, Vidall-Iglesias FJ, Liu YP, Wang XL. Preparation, characterization and catalytic performance of a novel Pt/SiC. *Electrochem Commun*. 2011;13(12):1309.
34. Shen XN, Zheng Y, Zhan YY, Cai GH, Xiao YH. Synthesis of porous SiC and application in the CO oxidation reaction. *Mater Lett*. 2007;61(26):4766.
35. Hatanaka M, Takahashi N, Takahashi N, Tanabe T, Nagai Y, Suda A, et al. Reversible changes in the Pt oxidation state and nanostructure on a ceria-based supported Pt. *J Catal*. 2009;266(2):182.
36. Jin JH, Li C, Tsang CW, Xu B, Liang CH. Catalytic combustion of methane over Pt–Ce oxides under scarce oxygen condition. *Ind Eng Chem Res*. 2016;55(8):2293.
37. Cargnello M, Doan-Nguyen VVT, Gordon TR, Diaz RE, Stach EA, Gorte RJ, et al. Control of metal nanocrystal size reveals metal–support interface role for ceria catalysts. *Science*. 2013;341(6147):771.
38. Lee J, Ryou Y, Chan XJ, Kim TJ, Kim DH. How Pt interacts with CeO_2 under the reducing and oxidizing environments at elevated temperature: the origin of improved thermal stability of Pt/CeO_2 compared to CeO_2. *J Phys Chem C*. 2016;120(45):25870.
39. Freund HJ, Meijer G, Scheffler M, Schlögl R, Wolf M. CO oxidation as a prototypical reaction for heterogeneous processes. *Angew Chem Int Ed*. 2011;50(43):10064.
40. Nagai Y, Hirabayashi T, Dohmae K, Takagi N, Minami T, Shinjoh H, et al. Sintering inhibition mechanism of platinum supported on ceria-based oxide and Pt–oxide-support interaction. *J Catal*. 2006;242(1):103.
41. Wu TX, Pan XQ, Zhang YB, Miao ZZ, Zhang B, Li JW, et al. Investigation of the redispersion of Pt nanoparticles on polyhedral ceria nanoparticles. *J Phys Chem Lett*. 2014;5(14):2479.
42. Zhou AB, Wang J, Wang H, Li H, Wang JQ, Shen MQ. Effect of active oxygen on the performance of Pt/CeO_2 catalysts for CO oxidation. *J Rare Earths*. 2018;36(3):257.
43. Peng RS, Li SJ, Sun XB, Ren QM, Chen LM, Fu ML, et al. Size effect of Pt nanoparticles on the catalytic oxidation of toluene over Pt/CeO_2 catalysts. *Appl Catal B*. 2018;220:462.
44. Liu HH, Wang Y, Jia AP, Wang SY, Luo MF, Lu JQ. Oxygen vacancy promoted CO oxidation over Pt/CeO_2 catalysts: a reaction at Pt–CeO_2 interface. *Appl Surf Sci*. 2014;314:725.
45. Damyanova S, Pawelec B, Arishtirova K, Huerta MVM, Fierro JLG. The effect of CeO_2 on the surface and catalytic properties of Pt/CeO_2–ZrO_2 catalysts for methane dry reforming. *Appl Catal B*. 2009;89(1–2):149.
46. Liao YN, He LF, Man CG, Chen LM, Fu ML, Wu JL, et al. Diameter-dependent catalytic activity of ceria nanorods with various aspect ratios for toluene oxidation. *Chem Eng J*. 2014;256:439.
47. Fan LJ, Xi K, Zhou Y, Zhu QL, Chen YF, Lu HF. Design structure for CePr mixed oxide catalysts in soot combustion. *RSC Adv*. 2017;7(33):20309.
48. Zhang DF, Zhang CS, Chen YM, Wang QF, Bian LY, Miao J. Support shape effect on the catalytic performance of Pt/CeO_2 nanostructures for methanol electrooxidation. *Electrochim Acta*. 2014;139:42.
49. Matam SK, Kondratenko EV, Aguirre MH, Hug P, Rentsch D, Winkler A, et al. The impact of aging environment on the evolution of Al_2O_3 supported Pt nanoparticles and their NO oxidation activity. *Appl Catal B*. 2013;129:214.